K&C Science Report – Phase 2

Operational rice monitoring & assessing rice paddy greenhouse gas emissions

William Salas
Applied Geosolutions
87 Packers Falls Rd
Durham, New Hampshire, USA 03857
Email: wsalas@agsemail.com
Ph: (603) 659-3363, Fax: (603) 659-0419

Collaborators
Nathan Torbick
87 Packers Falls Rd
Durham, New Hampshire, USA 03857

Cuizhen Wang
University of Missouri
Department of Geography
Columbia, Missouri, USA 65211

Yuan Zhang
College of Environment and Natural Resources
Zhejiang University
Hangzhou 310029, China

Xiangming Xiao
Department of Botany and Microbiology &
Center for Spatial Analysis
University of Oklahoma
Norman, Oklahoma, USA 73019

Changsheng Li
University of New Hampshire
Complex Systems Research Center
Durham, New Hampshire, USA 03857

Abstract- **Primary goals of JAXA's Kyoto and Carbon (K&C) Initiative are to utilize ALOS PALSAR to support conventions, carbon, and conservation science themes. During Phase 2 of the K&C Initiative we sought to operationalize a suite of rice monitoring algorithms to map rice extent and paddy agroecological attributes for sites in Asia and USA. We also carried out biogeochemical modeling simulations to assess the impact of rice managements on greenhouse gas emissions. Support Vector Machine and an operational thresholding approach that requires no a priori training data were applied. K&C SLT ScanSAR PALSAR strips, orthorectified ScanSAR images, and finebeam (FB) imagery were the primary data products used to support these activities during Phase 2. Field-level geophotos collected in China, India, Indonesia, and Thailand along with fine scale imagery were used as calibration and validation of the map products. Extensive preprocessing was carried out for Reference Path Systems (rsp) strips across regions of Monsoon Asia. Strip formatting structure and the complex nature of the K&C strips created computational and radiometric calibration challenges during pre-processing. Our results used PALSAR products to show the extent of rice for regions of Asia, the role of hydroperiod in influencing methane emissions, and the intensity of cropping cycles.**

***Index Terms*- ALOS PALSAR, K&C Initiative, rice, land use land cover, Monsoon Asia, biogeochemical modelling**

I. INTRODUCTION

A. Overview

Human modification of landscapes has been the foremost factor in wetland loss and degradation. Studies estimate that up to half of the world's wetlands have been lost due to human activities[1]. Demand for agriculture and land use development are the primary drivers influencing landscape modification trends. Rice paddies are a landscape feature that often gets considered to be a wetland land cover and an agricultural land use. Globally rice agriculture influences regional economies and global trade, health and food security, and the Earth system. Rice is the predominant food staple in many regions with more than several million tones in production annually with 95% of cultivation in developing regions. Rice land use globally is approximately 13048 million hectares and cultivation utilizes extensive human and natural resources[1].

Rice agriculture requires large resources through irrigation management and hydroperiod control. Rice hydroperiod is the flood frequency and duration of flooding for a paddy. The role of rice hydroperiod is poorly understood and potentially plays a large role in greenhouse gas emissions[3-6]. Methane (CH4) is one of the largest contributors to human-induced atmospheric change, second behind carbon dioxide. CH4 from rice accounts for 20% of global sources with irrigated rice accounting for 80% of rice CH4 emissions[6]. In order to more thoroughly monitor rice agriculture and land use changes improved methodologies and data products are needed.

In the past decade a number of studies have highlighted the advantages of L-band Synthetic Aperture Radar (SAR) for wetlands assessment. The primary advantages of L-band SAR data are its ability to penetrate canopies and sensitivity to vegetation structure, water content, and biomass independent of weather conditions. As part of the Japan Aerospace Exploration Agency (JAXA) Kyoto & Carbon Initiative, a PALSAR acquisition strategy has been developed with a goal of having spatially and temporally consistent data at continental scales with adequate revisit frequency and timing to enable the development of large-area products. The wetlands science team contributed to the development of the PALSAR acquisition strategy that includes ScanSAR data acquisitions of major wetlands regions every 46 days for regional mapping and characterization of aquatic ecosystems. Adjacent acquisitions overlap 50%, so effectively there are potentially 2 acquisitions every 46 days continuously starting from October 2006.

As part of JAXA's Kyoto and Carbon Initiative (K&CI), Applied Geosolutions, LLC (AGS) and colleagues applied operational mapping of rice ecosystems for large regions of Monsoon Asia and California, USA. In addition to the operational rice products, the team mapped land use land covers for regions of Monsoon Asia to improve monitoring and change analyses. This scientific progress report summarizes progress made by Applied Geosolutions during the JAXA K&CI Phase 2 activities during 2009~2010.

II. KYOTO AND CARBON INITIATIVE PHASE 2 FOCI

A. Relevance to the K&C drivers

The overarching themes of the JAXA K&CI are guided by the three **C**'s: **C**onventions, **C**arbon and **C**onservation. Under that guiding framework the rice and land use land cover mapping and modelling activities support projects to improve our understanding of human-environment interactions. During Phase 2 the activities and rice products have contributed to:

- Map rice paddies in an operational context;
- Assess the impacts of rice management decisions on methane and greenhouse gas emissions;
- Map disease 'hot-spots' and 'hot-times'
- Improve LULC datasets for scientists;
- Monitor agriculture and biogeophysical attributes

B. Sites

We primarily focused our K&C efforts on five sites during our recent K&C Phase 2 efforts. Analyses were conducted at multiple scales and included the use of various PALSAR products, including Slant Range ScanSAR strips, Orthorectified ScanSAR images, finebeam SLT strips, finebeam images, and optical imagery.

Study site 1. The Poyang Lake region, Jiangxi Province, China was a primary algorithm development site during Phase 1. During Phase 2 we operationalized the algorithms and validated products using field data from the region. Poyang Lake is the largest freshwater body in China and has significant ecological value. Multi-temporal ScanSAR (Red: DOY241, Green: DOY149, Blue: DOY103) WB1 (HH: 100m) display rice paddies (bright red) and other land use land covers in figure 1.

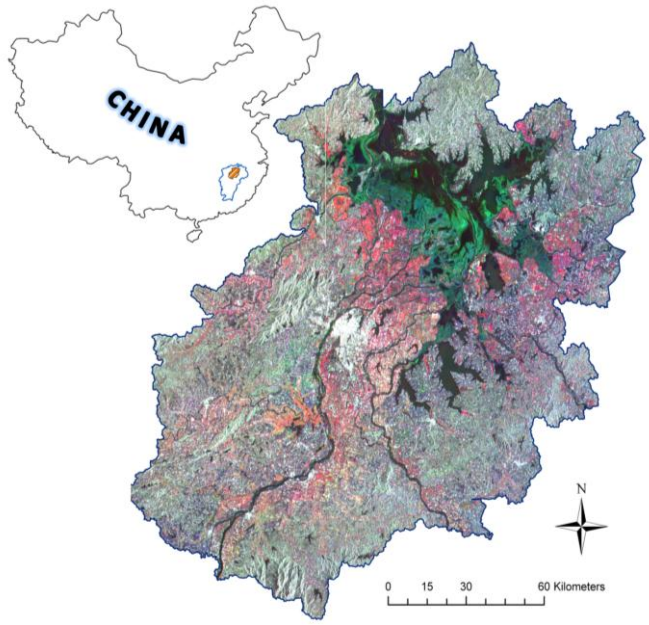

Figure 1: Multi-temporal ScanSAR data of Poyang Lake Watershed. Rice paddy areas appear as areas with various shades of red. The city of Nanchang is found near the center of the watershed (white area). Open water of Poyang Lake is the dark area.

Study site 2. During Phase 2 we utilized multitemporal (2009) SLT strips for large areas in Monsoon Asia with a focus on Thailand and Southeast China. The study is intended to understand the rate and magnitude of landscapes changes and the amount of rice agriculture. We carried out operational rice mapping for regions of Thailand, Laos, Cambodia and Vietnam. These information products are now being used to study land use changes by combining with decadal Landsat maps and climate models. Figure 2 presents an outline of the Countries for the rice study sites.

Study site 3. We used ALOS PALSAR to map LULC and rice agro-ecological patterns to help model highly pathogenic avian influenza (HPAI) across Java, Indonesia. HPAI hotspots occur where people, domestic poultry, and migratory waterfowl mix; often in rice paddies. The tropical island is approximately 132,000km^2 and is one of the world's leading rice producers with more than 50 million tones annually and 13 million hectares cultivated. The region has dramatic topographic changes and rice is grown at a variety of altitudes with a range of continuous crop cycles. The majority of rice paddies in Java are under some mechanism of irrigation control with only 10% considered rainfed lowlands. Large urban populations and coastal communities tend to cultivate *indica* subspecies. Paddies range from large-area commercial farms to terraced rice and isolated communities in the highlands creating a challenging rice mapping environments in this tropical climate. Better rice and LULC information help monitor potential HPAI hot-spots and hot-times. Figure 3 shows a mosaic of PALSAR data for study site 3.

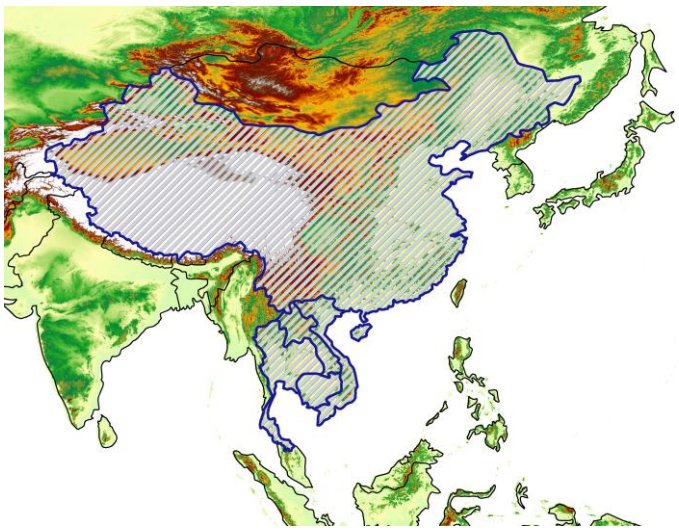

Figure 2: Study area for operational rice mapping. All major rice growing regions of the countries outlined were analyzed.

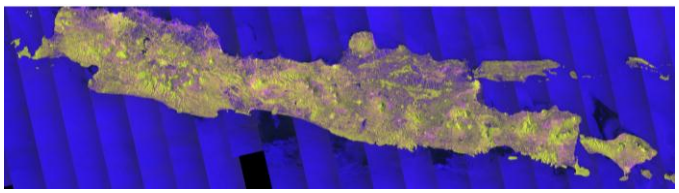

Figure 3 Study area for HPAI rice analysis. Island of Java, Indonesia was the study are for mapping rice attributes for HPAI risk modeling.

Study site 4. During Phase 2 we assessed the role of hydroperiod in greenhouse gas emissions for rice in California. Much of the rice grown in the USA is located in the northern Sacramento Valley of California (centered ~121.825W, 39.20N). Eight counties have substantial rice paddy agriculture include: Butte, Colusa, Glenn, Placer, Sacramento, Sutter, Yolo, and Yuba. Other dominant LULC classes in the region include sub/urban, natural vegetation, deciduous fruits and nuts, and field crops. Intensive irrigation and agricultural management occurs in the area. We used FBS, and ScanSAR images, and FBS strips products for the rice products and to parameterize a biogeochemical model. Figure 4 illustrates the location of study site 4.

Figure 4 California rice study area.

C. Approach

During Phase 2 we executed and tested two primary classification approaches to generate a suite of geospatial map products. The first approach included an operational decision tree that requires no a priori training data. The output products from the operational approach map rice extent, map hydroperiod, and generate metrics of cropping intensity and crop calendar. Initially operational algorithms were developed using FBS (HH, 12.5m spatial resolution) PALSAR images. Once the algorithms were designed they were scaled up and applied to ScanSAR strips. The simple decision-tree framework based on thresholding and tracking dynamics range of L-HH backscatter values was first used to identify rice paddies by capturing the characteristics of flooded areas and dynamic range representing rice phenology and harvest. Next, segmentation procedures are performed to create individual classified polygons of rice paddies. For each rice paddy, informative products were generated based on temporal dynamics of backscatter. Multi-temporal PALSAR is used to identify crop cycles, flood status, and phenology/biomass changes for each rice paddy. Empirical rice growth models and various post processing tools are used to refine those products Figure 5 illustrate the flow, logic and output products of the decision tree classification and processing system.

The second classification approach used Support vector machine (SVMs) framework. An SVM optimally discriminates any pair of classes by identifying a linear hyperplane that maximizes the distance between two training datasets. An SVM has several unique characteristics that are superior to conventional classifiers such as the maximum likelihood classifier (MLC) and artificial neural network (ANN). First, an SVM is not affected by the dimensionality problem for large satellite imagery. It effectively avoids overfitting of a training dataset by controlling the margin with the identification of a small subset of informative points, for example support vectors[9]. Consequently, SVMs have been applied successfully in land cover classifications with multitemporal, multifrequency, multipolarization SAR imagery[7-10]. Second, an SVM deals with noisy samples in a robust way. Camps-Valls et al.[7] reported that an SVM performed similarly for different training subsets with varying input dimension; for example, noises in training data were successfully detected and reduced in classification. Other studies also proved that, compared with conventional supervised classifiers, SVMs were more successful in processing noisy, heterogeneous multilayer data. Third, for classes that are not linearly separable in original image space, an SVM performs a kernel transformation to project raw data into a higher-dimension feature space. The classes in the new space become linearly separable and the margins between the classes are maximized[8]. For these reasons, an SVM could provide better accuracy in distinguishing paddy rice from other land uses.

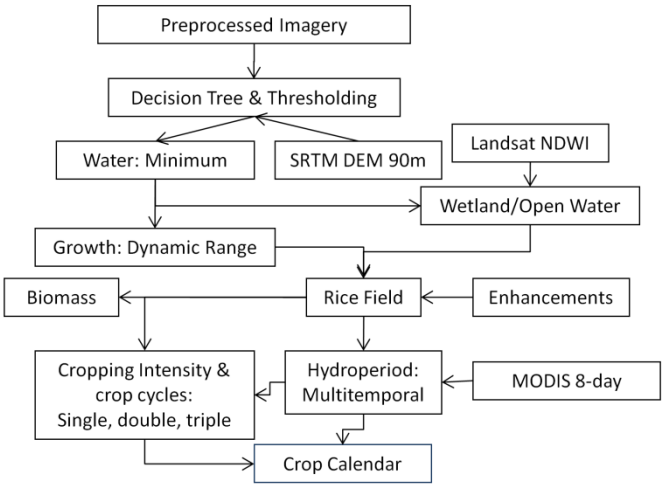

Figure 5.The product generation stream ingests fully pre-processed PALSAR imagery to provide spatially-explicit rice information products including biomass, crop cycles, and hydroperiod.

D. Satellite data

Slant Range ScanSAR

During this K&C period (2010) we focused on the utilization of Slant Range (SLT) ScanSAR strips for the study regions across Monsoon Asia and California. The primary regions of focus during Phase 2 period included Reference System for Planning (RSP) strips 91-115 covering Indonesia and China, RSPs 212-225 covering the pacific coast of the USA, and RSPs 106-139 covering Thailand and portions of neighboring peninsular countries of Cambodia, Laos, Myanmar, and Vietnam. Our archive of PALSAR strip products illustrated in Figure 6. Regions of Peninsular South East Asia and China have a large number of ScanSAR strips for 2006 to 2010.

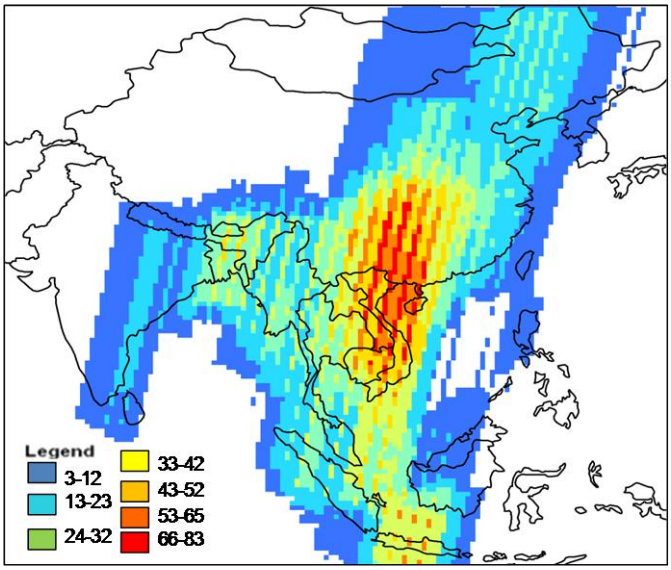

Figure 6. PALSAR image products pre-processed during Phase 2 for analysis and the number of overpasses for multitemporal mapping. Data cover 2006 to 2010.

The SLT ScanSAR imagery was preprocessed from native resolutions to radiometrically normalized and calibrated terrain geocoded strips. Raw SLT data was imported using orbit, doppler, and parameter files. Strips that observed similar geographic area underwent coregistration using a 4th order cubic convolution algorithm and SRTM DEM as input. Cross correlation windows had a range and azimuth size of 1024 and 4096, respectively, and a cross correlation grid threshold of 0.25. Fine shift parameters had range and azimuth sized windows of 32. These parameters were used due to the large coverage of the long ScanSAR strips.

All coregistered images underwent multitemporal filtering to reduce speckle or random multiplicative noise. An optimum weighting factor was applied to balance difference in signal across time. The data next were terrain geocoded following the range-Doppler approach as polynomials are inappropriate for SAR systems as nonlinear compression occurs. Imagery was radiometrically calibrated and normalized by eliminating local incident angle effects and antenna gain and spread loss patterns using an optimal resolution resampling approach. Local incidence angle and layover/shadow maps were generated for post classification processing to adjust for poor data pixels.

Fine-beam PALSAR

To train ScanSAR products and evaluate SAR-optical fusion techniques we utilized fine-beam PALSAR images including single (FBS), dual (FBD) and quad (PLR) polarization data. FB imagery was collected in Single Look Complex (SLC) to optimize the complete signal and adjust the effective number of looks considering the ground range resolution, the pixel spacing in azimuth, and incidence angle. FB data were co-registered using a cubic convolution cross-correlation approach considering shifts and range and azimuth dependency. Both de grandi and an anisotropic non-linear diffusion filter that adapts to target features were applied to further reduce speckle. Terrain geocoding used the best available digital elevation model (DEM) and followed the range-Doppler approach. FB data were radiometrically calibrated and normalized by eliminating local incident angle effects and antenna gain and spread loss patterns.

Orthorectified ScanSAR

Early during this K&C phase (2008-2009) we focused on the use of ground range orthorectified ScanSAR data as it was available for our study regions. These ScanSAR WB1 products (level 1.5) were processed using automated Python scripts that converted data into the desired products and formats for ingestion into a decision tree for monitoring land uses (see Torbick et al. [11]).

Landsat TM/ETM+

Landsat TM & ETM+ were used for moderate resolution fusion for mapping fine-scale rice and land cover attributes. The optical data provides information on canopy openness while the SAR data prodives information on vegetative structure, biomass, and land covers. Landsat data is now freely available from the USGS Global Visualization Viewer. The Landsat TM and ETM+ scenes were radiometrically converted from Digital Numbers (DN) to spectral radiance to top-of-atmosphere reflectance. Georeferencing examined noteworthy landscape features in a DEM and cross compared against the PALSAR imagery. Image gap masks were used in cases in which Scan Line Corrector (SLC) stripping caused missing data gaps.

NAIP Imagery

National Agriculture Imagery Program (NAIP) mosaics were utilized as ground control reference. NAIP data collection occurred near Day Of Year (DOY) 215 and 253 which is during the rice growing season at our USA sites. These true-color, 1-meter, digital photos are available through the United States Department of Agriculture (USDA) Geospatial Data Gateway. Data are compressed in MrSid format with a horizontal accuracy of less than 3 meters. Mosaics are tiled using a 3.75' x 3.75' quarter quads formatted to the UTM projection system using North American Datum 1983 (NAD83). Bounding coordinates covered the entire spatial domain that PALSAR imagery covered. Additional metadata are available via the USDA data gateway.

E. Challenges processing K&CI imagery

The relatively new formatting structure and complex nature of the K&C strips created computational and radiometric challenges during preprocessing. K&C strips cover large geographic areas extending over quite long latitudal zones. Strips often cover several hundred or a few thousand km. Multiple steps are required to process these images and thus a series of intermediate products are generated that require storage. Intermediate map products are generally 3-8 gigabits thus when developing products for large areas (ie, Monsoon

Asia) with multitemporal strips terabits of storage is required. During Phase 2 we generated more than 2 TB of preprocessed imagery for 2009 alone. Few commercial or open source software programs are adequate for processing these data. Therefore, we were required to develop a suite of executable Python program that we used combined with commercial and open source software to carry out pre-processing.

Absolute radiometric accuracy has been reported as <1.5dB between orbits[12] and the PALSAR strips are a significant advance in L-band information gathering. However, we did have some inconsistencies (antenna gain pattern and range spread loss) in persistent scattering targets were occasionally present when captured by different beams between orbits observed by adjacent paths (i.e., variation of 1 to 3.5 dB for consistent target) when using ORT image products. Correcting the unique K&C ScanSAR ORT image strips was also challenging. For an operational approach we executed a simplified normalization and calibration that used cross-correlation for adjacent RSP coregistration and operational thresholding of viewing geometry to reduce these inconsistencies and improve image quality. Effectively, the nearest and furthest beams of the ScanSAR strips had occasional noteworthy inconsistencies and were eliminated from our analysis.

F. Field campaign & reference data

An accuracy assessment was carried out and completed at Site 2. FBS rice paddy classifications and AUIG ScanSAR inundation status products were assessed for overall accuracy and misclassification patterns. A series of error matrices were constructed using the field-level data and high resolution color photography as reference.

For the FBS HH rice products a stratified random sampling scheme was utilized to insure statistical sampling rigor following well-established accuracy protocol. The validation scheme identified the maximum classified proportion to generate a specified sample number (475). A stratified random distribution with 250 rice points separated with a minimum distance of 300m was applied within the PALSAR rice product. A second suite of stratified random points were distributed among non-rice classes based on the ancillary LULC data from the Department of Water Resources (DWR) in California. Together these assessment data points provided 475 unique, statistically rigorous validation points. The accuracy points were checked using a variety of techniques. All points were compared against DWR LULC data and verified against the NAIP imagery

For the ScanSAR inundation status products a near-simultaneous field campaign was performed to assess the accuracy of the flood products at site 2. The overpass date was January 20, 2009. ScanSAR image scene centers were 40.464N x 120.379W and 37.991N x 120.977W. From the binary FBS rice maps two large clusters were chosen as focus areas for the winter flood assessment. The clusters were approximately 50km north of the City of Sacramento and 25km west of the City of Oroville. Ground truth data were collected using a GPS-enabled camera at approximately 1000m equal intervals following the road network. “Drive-by” transects were carried out and points were systematically collected within the two pre-selected clusters. GPS photos were collected perpendicular to the road direction using the stratified approach. A total of 130 points were collected for the second portion of the rice product assessment.

New field data collected during the 2010 campaign included ground truth from China, India, Indonesia, and Thailand. Geophotos (georeferenced digital photos) were collected using a stratified random sampling scheme at a suite of strategic locations in each country. Figure 7 provides some representative photos and illustrates the set of field photos locations for sites in Java, Indonesia. A set of stratified clusters along primary road networks were used to guide the geophotos collection campaign. *KML* (keyhole markup language) files were created to store and display points and photos on *Google Earth*. KML files use a tag based structure with attributes that allow display. These photos are available for viewing and sharing in *Google Earth* at http://www.eomf.ou.edu/ server. At this website users can search and share a library of global georeferenced field photos for product validation. Photos and land covers were interpreted at thousands of unique points with a focus on land covers of interest. For project regions focused on rice mapping we also collected numerous reference points at wetlands and riparian areas to evaluate typically misclassified patterns when mapping rice.

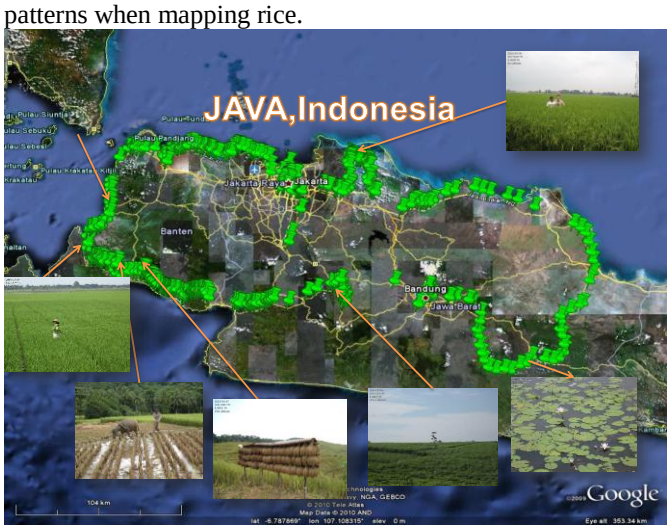

Figure 7. Example reference data collected using geophotos from field campaigns in China, India, Java, and Thailand.

G. Biogeochemical modelling

To assess GHG emission from rice paddies and land covers we used the process-oriented DeNitrification and DeComposition (DNDC) model[5,6]. This model was originally developed to simulate the effects of major farming practices (e.g., crop rotation, tillage, fertilization, manure amendment, irrigation, flooding, weeding, grass cutting and grazing) and

climate change (temperature and precipitation) on C and N cycles in various ecosystems. By tracking rice biomass production and decomposition rates, DNDC also simulates long-term soil organic carbon (SOC) dynamics, predicts CH_4 and N_2O emissions by tracking the reaction kinetics of nitrification, denitrification and fermentation across climatic zones, soil types, and management regimes.

Paddy soil is characterized by the frequent changes between saturated and unsaturated conditions driven by water management. During these changes in soil water content, the soil redox potential (i.e., Eh) is subject to substantial fluctuations between +600 and -300 mV. One of the key processes controlling CH_4 and N_2O production/consumption in paddy soils is soil Eh dynamics; CH_4 or N_2O are produced or consumed under certain Eh conditions (-300 to -150 mV for CH_4 and 200 to 500 mV for N_2O productions), so the two gases are produced during different stages of soil redox potential fluctuations. Regulated with the Nernst and Michaelis-Menten equations, DNDC tracks the formation and deflation of a series of Eh volume fractions driven by depletions of O_2, NO_3^-, Mn^{4+}, Fe^{3+}, and SO_4^{2-} consecutively, and hence estimates soil Eh dynamics as well as rates of reductive/oxidative reactions, which produce and consume CH_4 or N_2O in the soil. By tracking Eh dynamics, the model links the soil water regime to trace gas emissions for rice paddy ecosystems. DNDC predicts daily CH_4 and N_2O fluxes from rice fields through the growing and fallow seasons, as they remain flooded or shift between flooded and drained conditions.

This new DNDC model has been tested against several methane flux data sets from wetland rice sites in the U.S., Italy, China, India, Philippines, Thailand, and. Both CH_4 and N_2O fluxes were measured at five of the tested rice paddy sites where mid-season drainage was applied. A summary of many validation cases is shown in Figure 1, which demonstrates a fair agreement between observed and modeled CH_4 fluxes across a wide range paddy rice fields worldwide. The most recent validation work for California is indicated by the red (Maxwell site) and blue-green (RES: Rice Experiment Station, Biggs, CA) dots on Figure 1. The wide range in methane emissions for the California data are result of altered water and rice straw management which provides a sense of opportunities for reducing methane emissions. The results from the tests indicate that, with discrepancies for less than 20% of the tested cases, DNDC is capable of estimating the seasonal patterns and magnitudes of CH_4 and N_2O fluxes from the sites and is uniquely ready to serve mitigation analyses between C sequestration, N_2O and CH_4 emissions for rice agro-ecosystems.

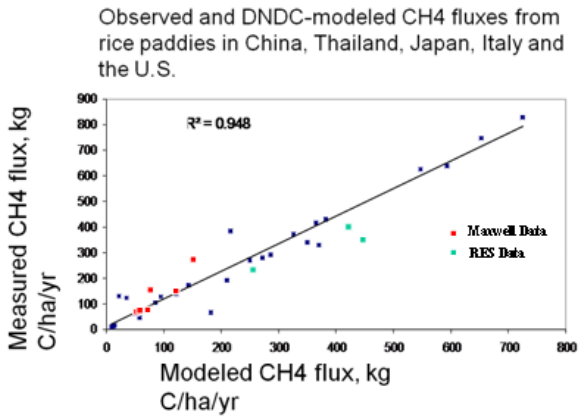

Figure 8: Independent validation of DNDC methane emissions. New sites were tested for the California rice sites based on field data collected by colleagues at UC Davis. Based on this validation, we are confident that DNDC provides good estimates of methane emissions from rice under several management regimes.

PALSAR rice products were used as spatial inputs for regional model simulations for all of California. In addition to the PALSR products, spatial database of soil and climate drivers were assembled for inputs for the model.We used the State Soil Geographic (STATSGO) database, which is a digital soil association map developed by the National Cooperative Soil Survey and distributed by the Natural Resources Conservation Service of the U.S. Department of Agriculture. It consists of a broad based inventory of. For climate data we used DAYMET daily weather data which is a models daily temperature, precipitation, humidity, and radiation over large regions of complex terrain.

III. Results and Summary

To streamline reporting results are summarized by project focus and region. Figure 5 illustrates the primary image processing steps and PALSAR products generated from the rice monitoring system.

A. Mapping Rice and Water Management in California Rice Fields

This section outlines the results of using PALSAR derived rice products for quantifying regional GHG emissions from rice paddies in California. PALSAR provided critical information on the extent of rice paddies and on the spatial and temporal dynamics of winter flooding. In the early 1990s, California banned the burning of rice straw for air quality improvements. As a result, famers began the practice of winter flooding to enhance winter decomposition of rice straw for better soil management. An added benefit of winter flooding was the creation of important wetland habitat along the Pacific Flyway for migratory waterfowl. A downside of the winter flooding is that additional methane is produced by anaerobic decomposition of the organic matter in the rice straw. The

timing, duration and patterns of winter flooding varies due to individual framer decisions, thus there is a need for mapping and monitoring.

1. Mapping rice extent in the Sacramento Valley, USA

The FBS data were used to delineate rice paddies according to the decision tree framework (i.e., threshold values) and overpass dates. The decision-tree identified nearly 155,000 hectares of rice paddies undergoing cultivation during the temporal FBS overpasses with an average patch size of 47 hectares. The FBS temporal windows (DOY of overpass) had a target of early and late development of the single rice crop system. In this region some rice fields are planted with off season cover crops and other managements to create habitat for migratory waterfowl. These factors created challenges for designing the decision tree metrics for temporal variation of backscatter from rice field during the offseason and were thus considered when creating and defining the rules within the decision-tree framework.

For a quantitative and application approach, image statistics generated from training polygons were identified as the optimal approach to define threshold rules. A set of rice training fields (comprised of ~40,000 known rice pixels) provided minimum, maximum, and dynamic range values for the decision tree threshold values. Average minimum, maximum, and range (σ^0) used were -22.6, -8.7, and 13.9, respectively. Table 1 illustrates examples statistics for 3 random fields. This approach provided a straight forward quantitative and operational approach to develop the decision tree rules with little a priori data. Our empirical values were compared with the field work in Inoue et al [12] .

Table 1. Three example rice training fields and associated image statistics for generating rice threshold values from flooded, peak maturation, and range. HH values are displayed in sigma naught (σ^0).

	Field 1	Field 2	Field 3
	Mean	Mean	Mean
Rice season (min)	-22.23	-22.90	-22.67
Rice season (max)	-10.08	-6.61	-9.52
Rice season (range)	12.15	16.29	13.15

ScanSAR data were used to map winter hydroperiod and inundation status for the 155,000 hectares of rice mapped. Each individual price paddy was characterized by presence of absence of winter flooding. If a paddy had winter flooding then the onset and duration of flooding were recorded. Figure 9 displays rice paddies and associated flood regimes near the Biggs Experimental Agricultural Station in the northern Sacramento Valley, California, USA. Approximately half of all rice paddies in the Sacramento Valley were flooded during a portion of the month of December. During Phase 1 image dates used were 12/5/2006, 3/7/2007, and 4/17/2007 to characterize a typical winter cycle. Approximately half of paddies (47% or 74,292 hectares) were flooded during December and 75% of rice paddies were flooded during at least one winter time period (table 2, fig 9).

Table 2. Study area *2* inundation status monitoring Approximately half of paddies (47% or 74,292 hectares) were flooded during **December** and 75% of rice paddies were flooded during at least one winter time period.

Hydroperiod	Area (hectares)	Percent
No Winter Flood	37866	24.4
Dec Flood	**74292**	**47.8**
Mar Flood	590	0.4
Dec & Mar Flood	11176	7.2
Apr Flood	8952	5.8
Dec & Apr Flood	17341	11.2
Mar & Apr Flood	159	0.1
Dec, Mar, Apr Flood	5083	3.3

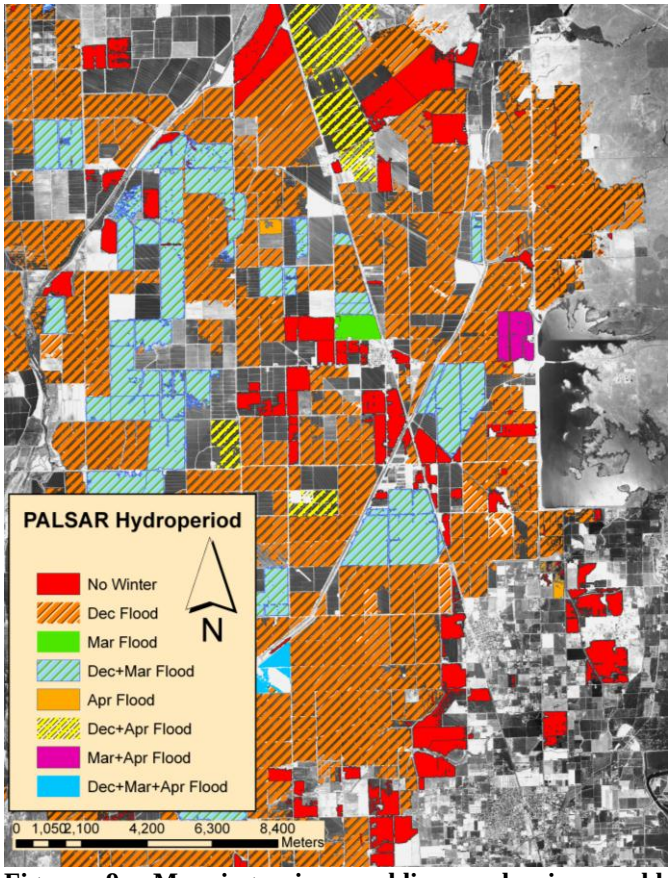

Figure 9. Mapping rice paddies and rice paddy hydroperiod with FBS and ScanSAR. Approximately 155,000 hectares of rice paddies were mapped in the rice growing season of 2007 in the Sacramento Valley, California, USA. Of these, approximately half (47%) were identified as flooded during December.

2. Accuracy of California, USA rice products

2a: Accuracy of rice mapping.

A field-campaign and ancillary reference information found the FBS HH rice paddy products to possess very high overall accuracy. The rice paddy map classification had an overall accuracy of 96% (449 / 469 = 0.9573). Given that 20 points were misclassified, the overall omission error was 0.0426. Kappa statistics had a khat value of 0.912609 with a variance and z-score value of 0.00036530 and 47.748, respectively with a p-value significance of <0.00001.

The misclassified points were distributed among five categories of errors. The majority of these errors were related to temporal challenges. This means that the rules used in the decision tree classifier to define the rice paddies eliminated a potential rice field due to shifts in flood cycles, harvest date, and/or overpass timing. Three errors were related to spatial problems where a point fell just outside a rice polygon or classified rice pixel. Three were related to confusion with dynamic wetland areas.

2b: Accuracy of mapping winter flooding.

Fieldwork was performed to assess the accuracy of the winter flood products for characterizing inundation status. Two ScanSAR scenes were processed and merged to complete coverage over the Sacramento Valley, USA. The overpass date was January 20, 2009. The field data were collected a in two clusters were approximately 50km north of Sacramento and 25km west of Oroville, respectively. Ground truth data were collected systematically using a GPS-camera at approximately equal intervals. Road transects were carried out and points were systematically collected. GPS-photos were collected perpendicular to the road every using the major routes bisecting the two clusters. Farmers implement winter flooding in different ways. Some food to a shallow depth and then till the soils, creating an uneven surface with clumps of rice straw and soil rising above the water surface. Other farmers till the crop residue into the soil and level the soils prior to flooding. This variability caused variability in backscatter from flooded fields. A total of 130 points were collected. Interpretation of the ground truth photos resulted in an overall accuracy of 96% (124/129). One point was thrown out due to error.

While PALSAR is not limited in imaging the surface under most conditions, the temporal frequency is limited by its 46 day repeat cycle. We assessed the added benefit of using MODIS to provide more temporal resolution to the timing of winter flooding onset and the duration of winter flooding which can have a significant impact of straw decomposition and GHG emissions. MODIS flood products (~500m) were evaluated by comparing them against four different ScanSAR flood maps. The comparison dates used the nearest MODIS 8-day interval. Therefore, ALOS overpass dates December 5, 2006, March 7 2007, April 17, 2007, and January 20, 2009 corresponded to MODIS DOY 2006339, 2007066, 2007107, and 2009020, respectively.

Generally, the flood products between the two sensors had strong agreement. Two by two contingency tables (i.e., binary flood vs. not flooded error matrices) resulted in agreements of 84-95%. The DOY 2006339 comparison had the most MODIS fill values (i.e., no data) with 28% of rice paddies containing portions of no fill pixels. The DOY 2009020 comparison had 251 rice paddies (8%) containing portions of no fill MODIS pixels. No fill values were filtered for the final comparisons resulting in a varying number of paddies compared at each interval. To evaluate the influence landscape configuration (namely size of individual paddies) and pixel size, all rice paddies under 50 hectares were withheld to assess accuracy of only larger fields. No statistically significant difference was found related to the size of paddies and accuracy in this study area.

The accurate rice products in this region then served as parameterization for the biogeochemical simulations using the DNDC model. Figure 10 illustrates simulations using the PALSAR-derived parameterizations (ie, inundation status and rice paddy). Results found that flooding regime decisions significantly impacts methane and greenhouse gas emissions.

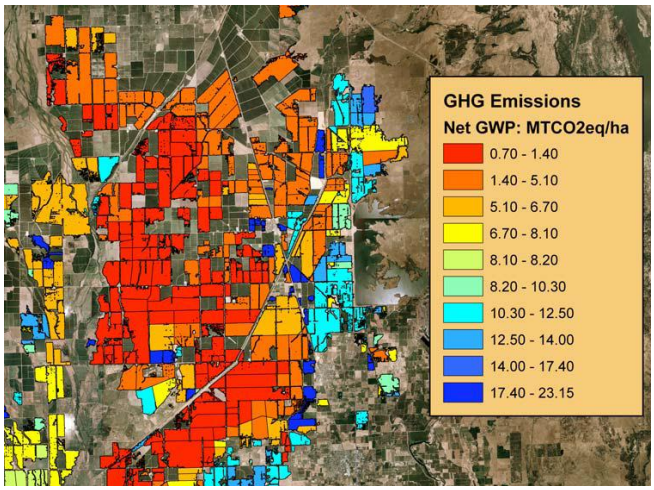

Figure 10. DNDC simulations uses PALSAR-derived rice information. Simulations found that flooding cycle decisions can substantially impact methane and GHG emissions.

B. Mapping watershed scale paddy rice in China & regional products in Monsoon Asia.

Our decision tree approach showed an effective ability to map rice agro-ecological paddy attributes at the site level. The first primary two nodes in the decision tree keyed off water and rice biomass growth using the preprocessed ScanSAR (refer to figure 5 for the decision tree logic). Average values from the training paddies using the multitemporal ScanSAR were obtained for the decision tree node to map rice extent.

The values (σ^0) used in the decision tree for minimum and maximum were -11 and -6.0, respectively, with dynamic range equal to the difference. To remove potential misclassifications the Landsat lake- and SRTM- masks were applied at the next node to eliminate topographic and wetlands confusion. At this stage in the decision tree the rice paddy extent map was created.

In the defined Poyang Lake Watershed (PLW), 5,862 km^2 were classified as rice paddies (fig. 11). This equates to approximately 25% of the watershed being classified as rice agriculture. The most intense regions of rice were adjacent to the southwestern coastline of the lake among tributaries of the Fuhe River and delta-like features of the Ganjiang River extending toward the City of Nanchang. Near-continuous rice paddies occupy the landscape immediately adjacent to the southeastern coastline among tributaries of the Xinjiang and Pojiang Rivers as well.

Jiang et al., (2008) classified approximately 45% of their PLW region as farmland in 2004 using Landsat imagery. Rao et al., (2002) classified approximately 40% land area as farmland. Jiang *et al* (2008) and Rao et al., (2002) combined rice with upload crops, such as orchards and vegetables, to reduce confusion; therefore, the different classification schemes are a noteworthy difference when comparing the findings from this study to other recent Poyang Lake region classifications. Considering differences in classifications scheme, objectives, data, and temporal and spatial scales, the proportional totals of the classified rice areas generated in this study are generally consistent with other recent classifications.

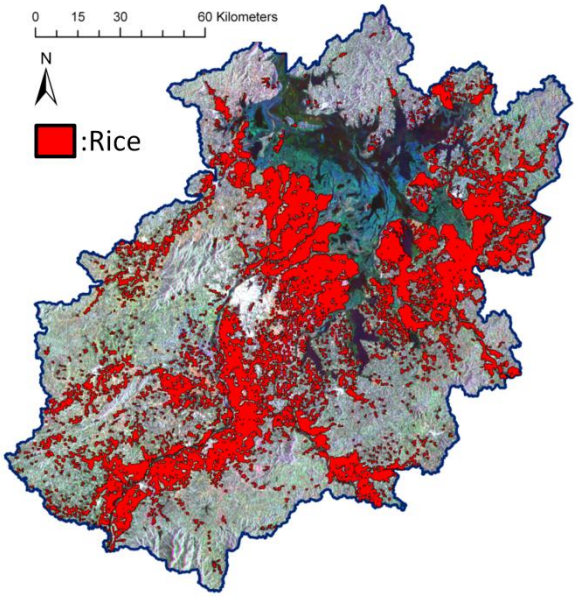

Figure 11. Rice (red) classification for the Poyang Lake watershed using multitemporal ScanSAR and Landsat water mask. An 89% overall accuracy was achieved according to georeferenced field photos.

From the ground truth field campaign a simple 2x2 binary matrix (rice vs. not rice) was generated to provide an overall accuracy for the rice map. We chose to carry out a simple contingency table as no other land covers were identified from the decision tree mapping rice paddy attributes. A total of 320 georeferenced field photos were categorized and an overall accuracy of 89% (286/320) was achieved. This represents a high overall accuracy considering the scale of the data and heterogeneous region classified. The high accuracy might be attributed to the fact that ground control points were stratified among aquatic habitats; however, these are most likely the types of land use/covers that would be most confused with rice paddies. It is possible that small and isolated rice paddies in higher elevation and more complex topography (which there is very little of in PLW) were under- or mis-classified. However, no anecdotal evidence showed this to be the case.

We believe the relatively high accuracy was achieved in part due to the PALSAR acquisition strategy and decision tree classifier. First, the multitemporal observations enable capturing key phenological patterns that are unique to rice. Few, if any, land types have patterns of growth and land management (i.e., flooding) that are similar to rice crops and its respective backscatter signal. The double bounce patterns of rice and erectly oriented aquatic vegetation with L-band SAR has been well established. Second, the Landsat water mask created during a high water event prevented numerous potential misclassifications due to dynamic lake wetland regions. While a small amount of rice paddies immediately adjacent to lake wetlands and riparian areas might have been under classified, the tradeoff in higher accuracy by eliminating misclassified coastal wetlands was desired. However, the georeferenced field photos provided no evidence that these regions were actually under classified. These results show that the operational approach can be executed with multi-temporal data acquired at the appropriate time relative to planting cycles with little to no a priori data to generate rice maps with multitemporal observations ScanSAR data.

Figure 12 illustrates the relationship between the paddy parameters and remote sensing metrics during a 'typical' double crop. Irrigation from canals precedes transplanting and the inundation status between crops within the same calendar year was shorter according to both the field measurements and remotely sensed hydroperiod metric. The figure indicates the inundation period between early and late rice in the double crop system was half as long (~two consecutive 8-day periods). In fact the hydroperiod for the initial flooding for early rice was eight consecutive 8-day periods at our corresponding field site; however, this figure begins closer to early crop transplanting as this is when field data collection began. MODIS flood pixels at site four began in day 73 and the paddy remained inundated until day 129 for a 56 day hydroperiod. As biomass increases the EVI signal increases, which, causes the LSWI signal to decrease. Once a biomass and EVI threshold are reached, the MODIS flood product has difficulty detecting water beneath maturing rice.

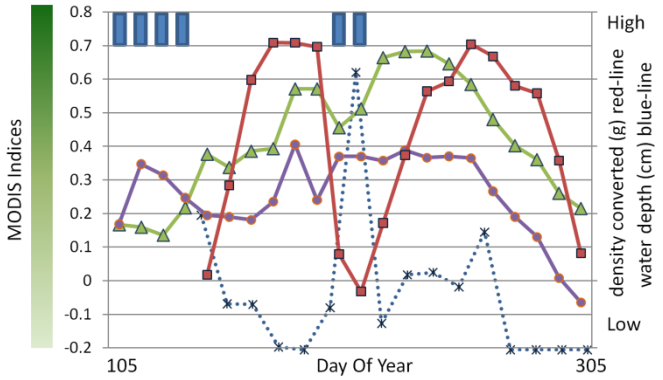

Figure 12. Data illustrating relationships between MODIS LSWI (purple line) and EVI (green line) indices, density-converted fresh haulm weight (biomass; red line), water depth (cm; dashed blue line) and hydroperiod (blue columns along top) over Day Of Year 105 to 325 (DOY) at Field site #4. Early rice was a slightly shorter crop compared to late rice in this double crop system. The flood product shows inundated paddy conditions during four and two consecutive 8-day indices preceding crops that generally correspond to rice phenology and water depth.

Biomass and water depth tended to be inversely related as expected. As the growing season progresses and rice matures water depth decreases toward harvest when paddies are fully drained. Some spikes in water depth are noted. Changes in water depth can be caused by a number of factors, including water management (e.g. frequency of water additions, soils, and evapotranspiration (ET) losses. Typically, farmers will flood fields to a depth of 10+ cm when they transplant rice. Overtime the depth of the water decreases due to leaching and ET losses. Depending on the rate of loss, farmers may or may not reflood before intentionally draining the field prior to harvest. The water depth and MODIS flood signal between early and late rice correspond well. As the paddy was flooded for the second crop in the double rice system, LSWI approached EVI to indicate flood conditions. In the longer flood period before early rice LSWI remained higher than EVI consistently.

While the amplitudes are slightly different, EVI and biomass appear generally related following similar trends. Some lag is apparent between EVI and the second rice crop at the illustrated field site. Some variability and noise are likely introduced when scaling from plot level data to MODIS pixels at 500m resolution and the fact that the composites are from a range of possible days over an 8-day period. The manmade bunds (primary "walls" separating main rice fields and irrigation channels) and the paddy checks (smaller secondary man-made "walls" within fields creating smaller paddies) that delineate fields into smaller, individual rice paddies contribute to mixed pixel issues at the 500m scale. Most likely isolated and patchy landscapes or terraced rice areas would be more challenging to monitor compared to large, near continuous scale paddies. The rice areas in the Poyang Lake Watershed primarily consist of large, contiguous fields (adjacent to lake and major tributaries), in flat geography, and undergoing similar managements which reduces mixed signal problems.

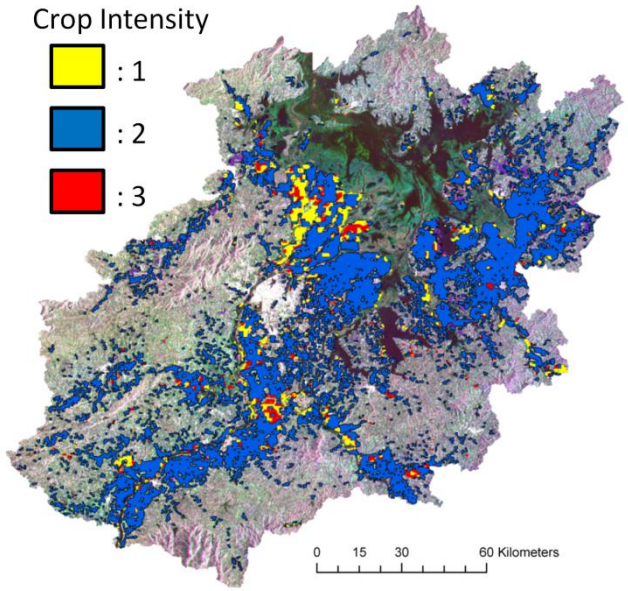

Figure 13. Map of rice cropping intensity (# of crops shown in legend) and unique hydroperiods for Poyang lake watershed. 85% of rice paddies were identified with two distinct inundated periods indicating double crop paddies.

After the rice extent node the high frequency MODIS was used to generate hydroperiod status at 8-day intervals for 2007. Approximately 85% of the rice paddies had two distinct hydroperiods, defined as at least two consecutive MODIS flood (LSWI+0.05>EVI) observations during the rice growing season (~DOY 81 to 329) in the watershed (fig 5). The 85% figure indicates that the majority of paddies were in a double crop intensity scheme. In other words, inundation periods are a signal of a crop cycles and two distinct and mutually exclusive inundation periods indicate a two crop pattern; an early crop and a late crop dominate rice management in the Poyang Lake Watershed. Four percent and three percent were found to be triple and single crop, respectively (see Figure 13). The operational approach executed here allowed for the continuous mapping of hydroperiod. This permits a better understanding of irrigation patterns and water resource.

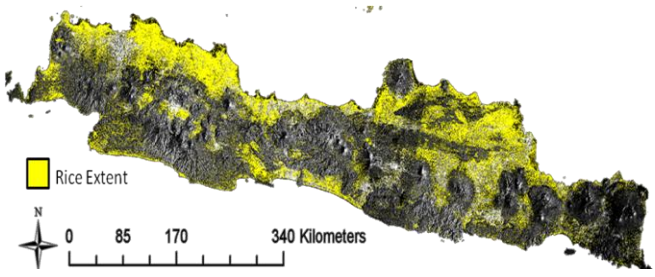

Figure 14. Regional Java maps created from multitemporal PALSAR ScanSAR to assist in modelling disease hot spots and hot times.

Dates for crop calendar monitoring using MODIS and ScanSAR covered observations between the DOY 80 to 330. Five ScanSAR observations were for DOY 103, 149, 190, 241, and 287. The MODIS observations covered 248 days with 31 8-day measurements using the start-end dates of 3/22/07 to 11/25/07. Using the rice extent node in the decision tree (see Figure 5), the thresholds were used to characterize phenological changes in rice paddies (measurements of rice growth, harvest, and flooding during the rice season). The temporal thresholds that were set created filters that did not allow erroneous crop and flood patterns. For example, rice crops take a period of time to grow (i.e., 90 days) and therefore multiple crops or flood signals cannot exist within a period less than a crop cycle (i.e., no 45 day crops). By temporally aggregating the number of crops and flood cycles the crop calendar was derived. The hydropeiod mapping approach that relies on high (temporal) frequency has been shown to be accurate in multiple rice ecosystems including Vietnam, China, and California, USA. Therefore, this operational approach can be executed for any region with no a priori data. Obtaining crop calendar field data of large regions is a challenge and future efforts will continue to ground truth calendar data.

We expanded the Poyang development and applied this approach to Java (Figure 14). Early qualitative results of these regional products has been fair (e.g. Java ~<75%); however, more radiometric calibration and strip to strip normalization is required for seamless information products. Early results applied to Thailand and neighbouring countries has also been challenging. The cause is likely due to the temporal frequency of the PASAR acquisitions relative to field looding, planting and harvest dynamics. In addition, it appears ScanSAR needs extensive processing and calibration for operational algorithms using no training data. We plan to address these issues during the current efforts at mapping rice paddies with finebeam strips and ScanSAR strips. We also to adjust the threshold values in our decision tree to perform a stepwise validation using several hundred field data points collected in Thailand and Java. We anticipate there will be trade-offs between User's and Producer's accuracies as we adjust the threshold criteria.

The scaling to continental products has been challenging with annual time series of ScanSAR. The graphics below (Figure 15) illustrates a region that contains a large area of paddies undergoing a similar cropping calendar for a region in Thailand. Scattered and smaller paddies are very challenging for ~75-100m ScanSAR due to the mixed signal. In addition the cropping calendar in regions where paddies are interspersed with field undergoing various stages of rice ag and managements creates more of a mixed signal.

C. Mapping paddy rice in Fuyang region China: Using Support Vector Machine algorithm for classification.

The PALSAR backscatter coefficient (σ°) images for different dates were stacked into a three-layer composite image. After upland hardwoods were masked out, the non-forest composite image was put in a Support Vector Machine (SVM) algorithm for a five-class thematic map was produced. Waterbodies were easily identified with clear boundaries. The urban area of Fuyang City was clustered in the upper center of the study area. The class map also demonstrated urbanization and intensified human settlement in lowland plains.

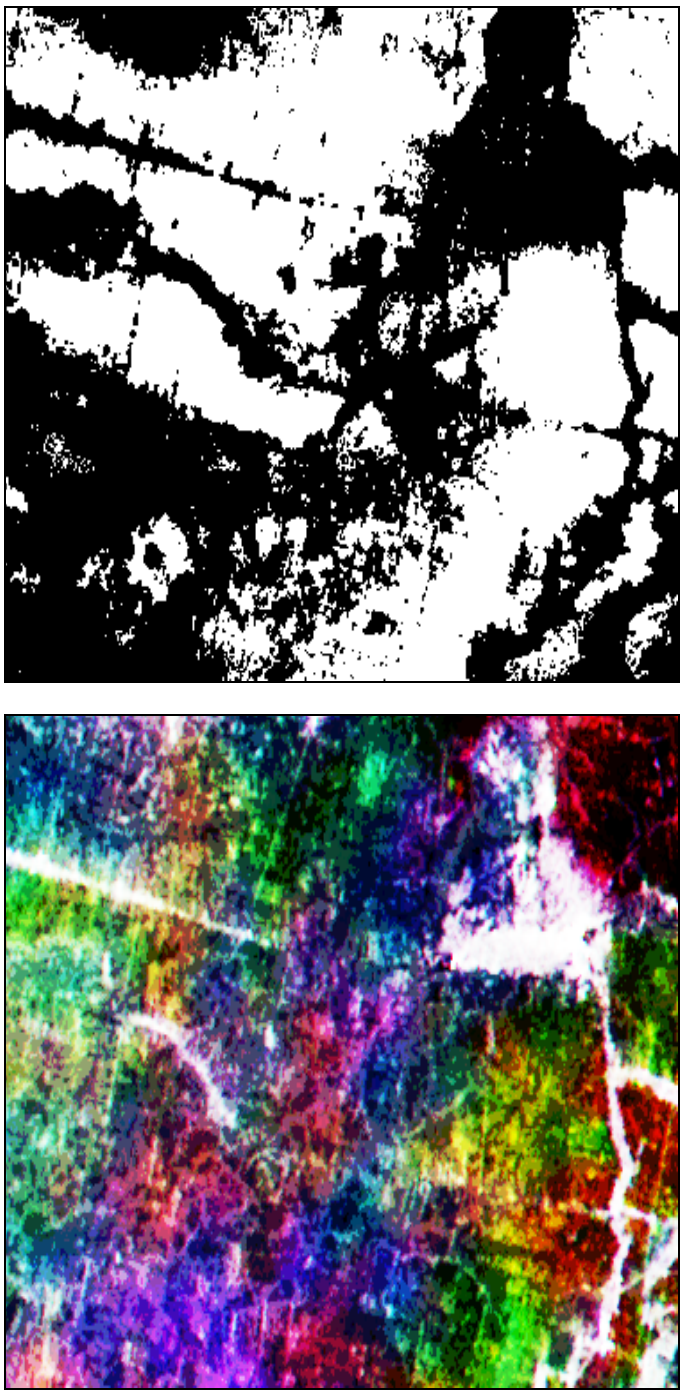

Figure 15. Multitemporal (R:3/28/09, G:5/13/09, B:9/28/09) SLT and rice extent map (top: white pixels) for rainfed paddies in near Khon Kaen, Thailand.

It was shown that rice planting was the major land use type in lowland plains in the study area. Large-area rice cultivation could be easily identified from PALSAR images. However,

except for the large flat plains along the Qiantang River in the middle of the study area, paddy rice fields were often small in size and fragmented with other land use surfaces. To demonstrate classification results of these small rice fields, a subset of class map was selected in the north of Xindeng Town, 30km southwest of urban core of Fuyang City (see Figure 16). Small rice fields were restricted by local topography and often clustered into narrow and long rice planting area. These areas were smaller and less continuous and resulted in a noisy and scattered pattern in the PALSAR class map. The under-classification of small rice fields was primarily caused by mixed pixels along field edges. These associated borders, however, were assigned rice in survey map because they were associated with rice cropping activities. In the subset, rice planting area detected in the PALSAR-derived map was 4.69×10^6 m^2 while the area in the census map was 5.13×10^6 m^2. Assuming survey map as ground truth, less than 10% of rice area was under-classified.

Two hundred (200) random points in each class were selected and served as validation sites to test the accuracy of the class map. At each validation site, the reference land use type was recorded from survey map. An error matrix of the five classes was built to compare ground-surveyed and image-classified results. The PALSAR class map in this area had an overall accuracy of 80.1% and Kappa statistics of 0.75. Paddy rice reached a user's accuracy of 90% and producer's accuracy of 76%. The relatively large commission error (24%) of rice mapping was primarily a result of misclassifying rice to dryland crop (19 out of 237) or orchard (16 out of 237). A large commission error also occurred where 21 out of 237 paddy rice fields were misclassified as water, a possible effect of open water in flooded rice fields. This may also partially result from land use change between PALSAR image acquisition (2006) and LULC ground survey (2005). For example, some rice fields in 2005 may be abandoned or converted to fish ponds in 2006. Nevertheless, the conditional Kappa value of paddy rice was 0.87, indicating that rice could be mapped at relatively high accuracy with multi-temporal PALSAR images.

With the remarkably high backscatter coefficients, urban structures were classified with the highest user's accuracy of 96.5% and conditional Kappa statistics of 0.95. Similarly, because of the very low backscatter, water surfaces were also easily classified with a user's accuracy of 80.5%. Some water bodies such as fishing ponds are small and shallow and sometimes covered with water vegetation, which contributed to large omission error (23.7%) of water surfaces. Dryland crops and orchards had the lowest accuracy (conditional Kappa value of 0.63 and 0.58, respectively), because of their backscatter similarity. Since the major objective of this portion of the research was rice mapping, the misclassification of these non-rice land uses was not investigated further.

Comparing with other SAR sensors, PALSAR has a great advantage in rice mapping[9]. Firstly, PALSAR has multi-mode imaging capabilities to acquire SAR imagery at varying resolutions and swaths, which provides flexible applications to fulfill tasks at various scale, extent and accuracies as well as costs. For example, the PALSAR images at FBS mode (6.25m pixel size) applied in this study could extract small and fragmented rice planting area, while the ScanSAR-mode images (100-m pixel size) could be more efficient in regional rice mapping. Among all SAR systems that are currently operating or operated in past years, only Radarsat-1/2 have the same multi-mode feature.

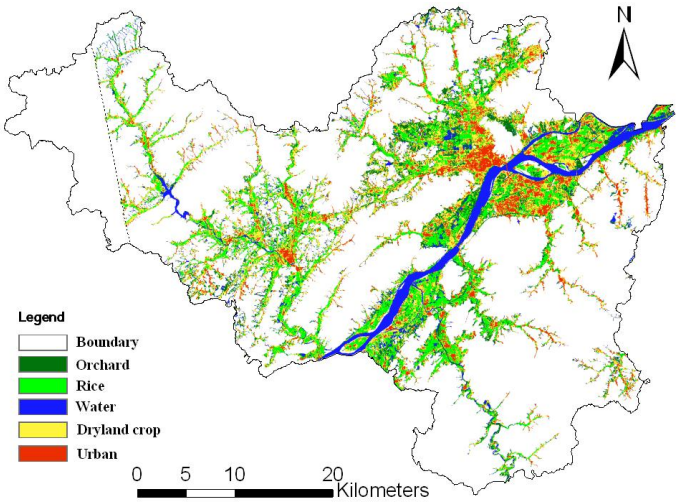

Figure 16. The class map derived from multi-temporal PALSAR images. The upland forest is masked out[9].

Secondly, PALSAR is the only sensor that could acquire imagery in multiple polarizations (HH, HV, and VV) and has a regional acquisition strategy for regional to continental mapping. Thirdly, as a successor of JERS-1 SAR, PALSAR is the only sensor that operates in relatively low frequency (L-band). L-band signals could penetrate deeper into rice canopy and therefore, may contain more information about total rice biomass than C-band signals of other systems. It has been demonstrated in past studies that different rice biophysical parameters were sensitive to backscatter in different polarizations and frequencies[10]. This information could be applied in radiative transfer models to quantify rice biophysical properties such as leaf area index and fresh biomass, which is closely related to rice production.

D. Ongoing efforts

We plan to focus on continuing the processing of the ScanSAR strips. Some of the earlier processed ScanSAR strips require adjacent strip calibration and more advanced products have been limited thus far as the number of overpasses within a single. Given the overall success of the ScanSAR acquisition strategy has resulted in significant gaps in the temoporal series of ScanSAR images and the relatively long revist time period with respect to rice phenology, we will examine integrating some FB strips into our processing stream to improve temporal frequencies and spatial resolution. We will apply these corrections to Monsoon Asia and California. In addition we will continue to merge mosaics and strips for improved mapping products in Monsoon Asia. We will test finebeam strips for Thailand and California as well. New field campaigns

(2011-2012) will be carried out in China, Thailand, and California.

ACKNOWLEDGEMENTS

This work has been undertaken within the framework of the JAXA Kyoto & Carbon Initiative. ALOS PALSAR data have been provided by JAXA EORC. Additionally support has been provided by JAXA, NASA LCLUC (#NNX08AL16G) and the National Institutes of Health (NIH). We also thank Francesco Holecz and the SARMAP team for collaborating and providing software assistance. We also thank our regional partners and the many local students who conducted field work.

REFERENCES

[1] Mitsch, W. and J. Gosselink. 2000. Wetlands, third edition. John Wiley & Sons, Inc., New York, NY, USA.

[2]International Rice Research Institute. World Rice Statistics. Statistical Database. http://irri.org.

[3]Li, C., S. Frolking, and T.A. Frolking, 1992a, A model of nitrous oxide evolution from soil driven by rainfall events: 1. Model structure and sensitivity, *Journal of Geophysical Research*, 97:9759-9776.

[4]Li, C., V. Narayanan, and R. Harriss, 1996, Model estimates of nitrous oxide emissions from agricultural lands in the United States, *Global Biogeochemical Cycles* 10:297-306

[5]Li, C., 2000, Modeling trace gas emissions from agricultural ecosystems, *Nutrient Cycling in Agroecosystems* 58:259-276.

[6]Li, C., J Qiu, S. Frolking, X. Xiao, W. Salas, B. Moore III, S. Boles, Y. Huang, and R. Sass, 2002. Reduced methane emissions from large-scale changes in water management in China's rice paddies during 1980-2000, *Geophysical Research Letters*, 29(20), doi:10.1029/2002GL015370, 2002.

[7]Camps-Valls, G., Go´ Mez-Chova, L., Calpe, J., Soria, E., Martin, J.D., Alonso, L. and Moreno, J., 2004, Robust support vector technique for hyperspectral data classification and knowledge discovery. IEEE Transactions on Geoscience and Remote Sensing, 42, pp. 1530–1542.

[8] Fukuda, J. and Hirosawa, H., 2001, Support vector machine classification of land cover: application to polarimetric SAR. In Proceedings of the International Geoscience and Remote Sensing Symposium (IGARSS), 9–13 July, Sydney, Australia (Piscataway, NJ: IEEE), pp. 187–189.

[9] Angiulli, G., Barrile, V. and Cacciola, M., 2005, SAR imagery classification using multiclass support vector machines. Journal of Electromagnetic Waves and Applications, 19, pp. 1865–1872.

[10] Tan, C.P., Koay, J.Y., Lum, K.S., Ewe, H.T. and Chuah, H.T., 2007, Classification of multitemporal SAR images for rice crops using combined entropy decomposition and support vector machine technique. Progress in Electromagnetics Research (PIER), 71, pp. 19–39.

[11] Torbick, N., Salas, W., Hagen, S., Xiao, X. 2010. Mapping rice agriculture in the Sacramento Valley, USA with multitemporal PALSAR and MODIS imagery. IEEE J. Selected Topics in Remote Sensing. DOI 10.1109/JSTARS.2010.2091493.

[12.] Rosenqvist, A., Shimada, S., Watanbe, M. 2004. ALOS PALSAR: Technical outline and mission concepts. 4th International Symposium on Retrieval of Bio- and Geophysical Parameters from SAR Data for Land Applications, Innsbruck, Austria, November 16-19, 2004.

JAXA K&CI PI.

William A. Salas is President and Chief Scientist of Applied Geosolutions, LLC in New Hampshire, USA. Dr. Salas has degrees in mathematics, forestry, and natural resources from the Universities of Vermont and New Hampshire, respectively. He formed AGS in the year 2000 to promote, support and provide scientifically sound cutting-edge geo-spatial technologies, biogeochemical modeling applications, and integrated spatial information services. AGS works with private companies, universities, governments, NGOs, and federal agencies.

Collaborators.

Nathan Torbick is a Research Scientist at Applied Geosolutions In New Hampshire, USA. Dr. Torbick joined AGS after completely his graduate work at the Center for Global Change and Earth Observation at Michigan State University. His research foci are human-environment interactions, aquatic ecosystem assessment, and geospatial technologies.

Xiangming Xiao earned a Bachelor's degree in Biology from Xiamen University, China in 1982, and a Master's degree in Plant Ecology from Institute of Botany, Chinese Academy of Science and University of Science and Technology, China in 1987, and a UNEP/UNESCO's Diploma of Environmental Management and Protection from University of Technology, Dresden, Germany in 1988, and a Ph.D degree in Ecosystem Science from Colorado State University in 1994. Dr. Xiao recently began a new position at the University of Oklahoma after working at the Complex Systems Research Center at the University of New Hampshire. His research interests span a wide range of biological science, geo-science and health science, including climate change, land use and land cover change, global carbon cycle, remote sensing, and epidemiology and ecology of infectious diseases.

Changsheng Li received his Bachelor's degree in Geochemistry from University of Science and Technology of China in 1964, Master's degree in Environmental Chemistry from Chinese Academy of Sciences in 1981, and Ph.D. degree in Biogeochemistry from Chinese Academy of Sciences and University of Wisconsin in 1985. He has been devoted to biogeochemical and environmental studies since. In 1992 he moved to the University of New Hampshire where he is now Research Professor in the Complex Systems Research Center within the Institute for the Study of Earth, Oceans, and Space. His academic interest is to explore the theories and methodologies which can be used for revealing relationship between humankind and their environment. Dr. Li has been focusing his study on biogeochemical cycling of chemical elements, especially its numerical expression in time and space.

Chuizhen Wang is an Assistant Professor at the University of Missouri in the Department of Geography. Chuizhen joined UM after completing her PhD at Michigan State. Dr. Wang's primary research areas are bio-environmental remote sensing, GIS and spatial analysis. Particular interests are in biodiversity, biophysical retrieval, ecosystem and environmental mapping. Her past research experience includes Land Use/Land Cover mapping, canopy radiative transfer modeling, and quantitative biophysical estimation with optical and microwave remotely sensed data.

Zhang Yuan received the B.S. degree from Liaoning Normal University, China, in 1998, and the M.A. degrees in Dept. of Forestry, Sheyang Agricultural University, China, in 2003. He is currently a Ph.D candidate in the Institute of Agricultural Remote Sensing and Information Technology Applications, Zhejiang University, China. His research interests are in biophysical and environmental remote sensing and ecosystem simulation.